Journal of Dental Research
2017, Vol. 96(1) 81–91

DOI: 10.1177/0022034516663633
jdr.sagepub.com

# Conditional *Alpl* Ablation Phenocopies Dental Defects of Hypophosphatasia

**B.L. Foster[1*], P. Kuss[2*], M.C. Yadav[2], T.N. Kolli[1], S. Narisawa[2], L. Lukashova[3], E. Cory[4,5], R.L. Sah[4,5,6], M.J. Somerman[7], and J.L. Millán[2]**

**Abstract**

Loss-of-function mutations in *ALPL* result in hypophosphatasia (HPP), an inborn error of metabolism that causes defective skeletal and dental mineralization. *ALPL* encodes tissue-nonspecific alkaline phosphatase, an enzyme expressed in bone, teeth, liver, and kidney that hydrolyzes the mineralization inhibitor inorganic pyrophosphate. As *Alpl*-null mice die before weaning, we aimed to generate mouse models of late-onset HPP with extended life spans by engineering a floxed *Alpl* allele, allowing for conditional gene ablation (conditional knockout [cKO]) when crossed with *Cre* recombinase transgenic mice. The authors hypothesized that targeted deletion of *Alpl* in osteoblasts and selected dental cells (*Col1a1*-cKO) or deletion in chondrocytes, osteoblasts, and craniofacial mesenchyme (*Prx1*-cKO) would phenocopy skeletal and dental manifestations of late-onset HPP. *Col1a1*-cKO and *Prx1*-cKO mice were viable and fertile, and they did not manifest the epileptic seizures characteristic of the $Alpl^{-/-}$ model of severe infantile HPP. Both cKO models featured normal postnatal body weight but significant reduction as compared with wild type mice by 8 to 12 wk. Plasma alkaline phosphatase for both cKO models at 24 wk was reduced by approximately 75% as compared with controls. Radiography revealed profound skeletal defects in cKO mice, including rachitic changes, hypomineralized long bones, deformations, and signs of fractures. Microcomputed tomography confirmed quantitative differences in cortical and trabecular bone, including decreased cortical thickness and mineral density. *Col1a1*-cKO mice exhibited classic signs of HPP dentoalveolar disease, including short molar roots with thin dentin, lack of acellular cementum, and osteoid accumulation in alveolar bone. *Prx1*-cKO mice exhibited the same array of periodontal defects but featured less affected molar dentin. Both cKO models exhibited reduced alveolar bone height and 4-fold increased numbers of osteoclast-like cells versus wild type at 24 wk, consistent with HPP-associated periodontal disease. These novel models of late-onset HPP can inform on long-term skeletal and dental manifestations and will provide essential tools to further studies of etiopathologies and therapeutic interventions.

**Keywords:** bone biology, cementum, dentin, periodontal tissues/periodontium, mineralized tissue/development, tooth development

## Introduction

*ALPL* encodes tissue-nonspecific alkaline phosphatase (TNAP), an enzyme expressed in bone, teeth, liver, and kidney (Millán 2006). TNAP hydrolyzes the mineralization inhibitor inorganic pyrophosphate and dephosphorylates pyridoxal 5′-phosphate, the major circulating form of vitamin B6, among other substrates. Loss-of-function mutations in *ALPL* result in hypophosphatasia (HPP), an inborn error of metabolism that causes defects in skeletal and dental mineralization (Millan and Whyte 2016; Whyte 2016). The broad range of HPP manifestations spans from severe life-threatening forms (infantile and perinatal) to milder forms (prenatal benign, childhood, adult, and odontohypophosphatasia). Skeletal defects include rickets, osteomalacia, fractures, and bone pain. Dental manifestations include cementum deficiency, tooth loss, thin dentin, enamel alterations, and periodontal disease (Foster, Nociti, et al. 2014; Foster, Ramnitz, et al. 2014). Dental hard tissues are exceptionally sensitive to HPP, as all clinical forms of HPP feature dentoalveolar defects, with odontohypophosphatasia affecting only the dentition (Bloch-Zupan 2016).

The *Alpl* knockout ($Alpl^{-/-}$) mouse model phenocopies severe infantile HPP, including early postnatal onset; skeletal manifestations, including rickets and osteomalacia; and vitamin B6–dependent seizures found in only the most severe cases of perinatal and infantile human HPP (Narisawa et al.

[1]Division of Biosciences, College of Dentistry, The Ohio State University, Columbus, OH, USA
[2]Sanford Children's Health Research Center, Sanford Burnham Prebys Medical Discovery Institute, La Jolla, CA, USA
[3]Hospital for Special Surgery, New York, NY, USA
[4]Department of Bioengineering, University of California–San Diego, La Jolla, CA, USA
[5]Center for Musculoskeletal Research, University of California–San Diego, La Jolla, CA, USA
[6]Department of Orthopaedic Surgery, University of California–San Diego, La Jolla, CA, USA
[7]National Institute of Arthritis and Musculoskeletal and Skin Diseases, National Institutes of Health, Bethesda, MD, USA
*Authors contributing equally to this article.

A supplemental appendix to this article is published electronically only at http://jdr.sagepub.com/supplemental.

**Corresponding Author:**
J.L. Millán, Sanford Burnham Prebys Medical Discovery Institute, 10901 N. Torrey Pines Road, La Jolla, CA 92037, USA.
Email: millan@sbpdiscovery.org

1997; Fedde et al. 1999). Defects in cementum, dentin, alveolar bone, and enamel have been demonstrated in *Alpl*$^{-/-}$ mice (McKee et al. 2011; Foster et al. 2012; Yadav et al. 2012; Foster, Nagatomo, et al. 2013; Zweifler et al. 2015). However, these mice die by 2 to 3 wk of age, thereby preventing analysis of HPP-associated pathologies at advanced ages.

We aimed to generate additional mouse models of late-onset HPP with extended life spans. Our approach was to create a mouse harboring a floxed *Alpl* allele, allowing for conditional gene ablation when crossed with different *Cre* recombinase deleter mice. We hypothesized that targeted deletion of *Alpl* in osteoblasts and selected dental cells (*Col1a1*-cKO [conditional knockout]) or deletion in chondrocytes, osteoblasts, and craniofacial mesenchyme (*Prx1*-cKO) would phenocopy skeletal and dental manifestations of HPP but without epileptic seizures that herald early lethality.

## Materials and Methods

### Mice

Animal studies were approved by the Sanford Burnham Prebys Medical Discovery Institute Institutional Animal Care and Use Committee. Creation of floxed *Alpl* (*Alpl*$^{fl/fl}$) mice on a C57BL/6 genetic background is described in the Appendix. Tg(Col1a1-cre)2Bek/Mmusd (Mutant Mouse Resource and Research Centers [MMRRC], University of California–Davis) mice harboring the *Col1a1-Cre* transgene (Cre recombinase under control of the *Col1a1* 2.3-kb promoter) have been described (Dacquin et al. 2002). B6.Cg-Tg(Prrx1-cre)1Cjt/J (The Jackson Laboratories) harboring the *Prx1-Cre* transgene have also been described (Logan et al. 2002). Mice heterozygous for the floxed allele (*Alpl*$^{fl/+}$) were crossed with Cre deleter mice to generate *Col1a1-Cre*$^{+}$*;Alpl*$^{fl/fl}$ (*Col1a1*-cKO) or *Prx1-Cre*$^{+}$*;Alpl*$^{fl/fl}$ (*Prx1*-cKO) mice (homozygous for floxed allele knockout). Wild-type (WT) controls included *Alpl*$^{fl/fl}$ and *Cre*$^{+}$;*Alpl*$^{wt/wt}$ littermates. Skeletons were harvested at 24 wk and fixed in 4% paraformaldehyde ($n$ = 2 to 4 for all genotypes).

### Plasma Chemistry Analysis

After anesthesia with Avertin (0.017 mL/g body weight), blood was collected by cardiac puncture and transferred to lithium-heparinized tubes (Becton; Dickinson & Co.), and plasma was separated by centrifugation at 5,000 rpm for 10 min. Plasma alkaline phosphatase (ALP) activity was measured as previously described (Millán et al. 2008).

### Radiography

Radiography of the skeleton was performed with an MX20 Specimen Radiograph System (Faxitron X-ray Corporation). Hemimandibles were scanned in a cabinet x-ray (Faxitron X-ray Corporation) at 30 kV for 40 s.

### Micro–Computed Tomography

Detailed methods for micro–computed tomography (micro-CT) analyses of skeletal elements are described in the Appendix. For skeletal analysis, samples were scanned on a Skyscan 1076. Cortical bone analyses included cross-sectional tissue area (T.Ar), cross-sectional cortical bone area (B.Ar), cortical bone area fraction (B.Ar/T.Ar), cross-sectional bone thickness, cortical porosity, polar moment of inertia, and tissue mineral density (TMD). Trabecular bone analyses included tissue volume (TV), trabecular bone volume (BV), trabecular bone volume fraction (BV/TV), trabecular thickness, trabecular separation, trabecular number, structure model index, trabecular pattern factor, and bone mineral density (Bouxsein et al. 2010; Yadav et al. 2011).

For dentoalveolar analysis, dissected hemimandibles were scanned on a Scanco Medical microCT 35 (Scanco Medical AG). Scanning parameters were 6-µm voxel size, 55 kVp, 145 mA, with 0.36° rotation step (180° angular range), and a 400-ms exposure per view. Digital Imaging and Communications in Medicine (DICOM) files were reoriented through ImageJ software (1.48r), with comparable coronal and sagittal cut planes chosen for image comparison. DICOM stacks were rendered as 3-dimensional isoimages with Drishti 2.6.1 (https://github.com/AjayLimaye/drishti; Limaye 2012). Dentoalveolar analyses included TV, BV, BV/TV, TMD, and dentin thickness.

### Histology and Immunohistochemistry

Skeletal and dentoalveolar tissues used for histology were fixed in 4% paraformaldehyde. Skeletal histology and histomorphometry (including undecalcified sample preparation) are described in the Appendix. Mandibles were demineralized in AFS solution (acetic acid, formaldehyde, sodium chloride) and embedded in paraffin for 6-µm serial sectioning, as described previously (Foster 2012). Deparaffinized dentoalveolar sections were stained by hematoxylin and eosin or picrosirius red (Foster 2012). Staining was performed for tartrate-resistant acid phosphatase (TRAP) to identify osteoclasts (Foster, Soenjaya, et al. 2013; Wako Chemicals). Immunohistochemistry was performed on deparaffinized sections with rat monoclonal anti-human TNAP (R&D Systems; Zweifler et al. 2015) and an avidin-biotinylated peroxidase-based kit (Vectastain Elite; Vector Labs) with a 3-amino-9-ethylcarbazole substrate (Vector Labs).

### Statistical Analysis

Results are expressed as mean ± SD. Data were analyzed with Student's $t$ test (independent samples) where $P$ values <0.05 were considered statistically significant.

## Results

### *Conditional Deletion of* Alpl *Results in Late-Onset HPP*

Mice harboring a floxed *Alpl* allele (*Alpl*$^{fl/fl}$) were crossed with *Cre* deleter mice to direct selective deletion in desired tissues. For skeletal analysis, *Col1a1-Cre* mice were used to target *Alpl* deletion to osteoblasts (Dacquin et al. 2002), while *Prx1-Cre* mice were used to target *Alpl* deletion to early limb bud mesenchyme, including osteoblasts and chondrocytes (Logan et al.

2002). *Col1a1-Cre;Alpl*$^{fl/fl}$ (*Col1a1*-cKO) and *Prx1-Cre;Alpl*$^{fl/fl}$ (*Prx1*-cKO) mice were viable and fertile, and they did not undergo epileptic seizures characteristic of *Alpl*$^{-/-}$ mice (Waymire et al. 1995; Narisawa et al. 1997). *Alpl*$^{-/-}$ mice featured >50% reduction in weight by 1 wk, nearly undetectable plasma ALP, and multiple organ abnormalities. In contrast, these cKO models featured normal postnatal body weight at early ages, with significant reduction observed at 8 wk for *Prx1*-cKO and 12 wk for *Col1a1*-cKO as compared with WT (Fig. 1A, B). At 24 wk, both cKO mice had approximately 50% the weight of controls. Plasma ALP for both cKO models was reduced by approximately 75% versus controls, as measured at 24 wk (Fig. 1C).

Radiography of *Col1a1*- and *Prx1*-cKO skeletons revealed profound defects (femora shown in Fig. 1D–F and additional bones shown in Appendix Fig. 1), including radiolucency of skeletal elements, thin cortical bone, twisted and deformed long bones with signs of fractures and callus formation, deformed vertebrae, and features consistent with rickets, such as disorganized growth plate regions, widened ends, and reduced length of long bones (described in more detail in the Appendix and shown in Appendix Figs. 1–4). *Prx1*-cKO mouse long bones appeared more severely affected than those of *Col1a1*-cKO mice, exhibiting more obvious reductions in size, deformations in shape, growth plate disturbance, and surface degradations and lesions.

Micro-CT analysis identified altered cortical midshaft bone and metaphyseal trabecular bone of humeri, femora, and tibiae in both *Col1a1*- and *Prx1*-cKO mice (femora shown in Fig. 1G–R with additional bones shown in Appendix Figs. 2–4). Cortical bone was altered in all 3 bones of both cKO models, with a 29% to 40% decrease in cross-sectional bone thickness versus WT and with *Col1a1*-cKO mice presenting a greater number of significant changes in cortical bone than *Prx1*-cKO mice (Appendix Table 1). Additionally, there were trends for reduced B.Ar, B.At/T.Ar, and TMD when compared with WT (not all $P < 0.05$). Trabecular bone in metaphyses was also altered in all 3 bones of both cKO models, with variable trends between models and across sites (Appendix Table 2). Generally, when compared with WT, there were increases in TV and trabecular separation and decreases in trabecular pattern factor and bone mineral density in both cKO mice. Micro-CT results are discussed in more detail in the Appendix.

Undecalcified sections of humeri, femora, tibiae, and vertebrae were stained by von Kossa and van Gieson assays and analyzed by histomorphometry software (Appendix Fig. 5), revealing significantly reduced relative bone volume for all bones, as well as significantly increased ($P < 0.05$) or trends for increased ($P > 0.05$) osteoid volume in both cKO models. Disturbed growth plate regions, especially in *Prx1*-cKO humeri, supported rachitic changes.

## *Dentoalveolar Defects in* Alpl *cKO Mice*

Given the skeletal phenotypes, we suspected dentoalveolar involvement and analyzed these tissues in cKO mice. As dentoalveolar tissues were analyzed only at 24 wk, potential effects of *Alpl* ablation on tooth eruption were not evaluated in the current study. In dentoalveolar tissues, *Col1a1-Cre* deleter mice direct ablation to osteoblasts, odontoblasts, cementoblasts, and fibroblasts (Dacquin et al. 2002; Liu et al. 2014). Cranial radiographs indicated normal anatomy and dental occlusion in *Col1a1*-cKO mice (Fig. 2A, B). However, radiography of hemimandibles revealed that, when compared with WT, *Col1a1*-cKO mice exhibited hypomineralization of mandibular bone, short molar roots with thin dentin, and delayed root dentin in the incisor (Fig. 2C, D). Two-dimensional micro-CT analysis confirmed thin molar root dentin and widened pulp chambers, reduced alveolar bone, and severely dysmorphic incisor root dentin (Fig. 2E–L). Quantitative micro-CT analysis confirmed statistically significant reductions in *Col1a1*-cKO alveolar bone BV, BV/TV, and TMD (Appendix Table 3). While crown dentin did not exhibit significant differences from WT, *Col1a1*-cKO root dentin BV, BV/TV, TMD, and thickness were significantly reduced versus WT. Three-dimensional reconstructions confirmed dramatically reduced alveolar bone height in *Col1a1*-cKO mice (Fig. 2M, N).

Histology showed thin dentin, lack or reduction of acellular cementum, periodontal ligament (PDL) detachment, apical migration of junctional epithelium, reduced alveolar bone, and osteoid accumulation in *Col1a1*-cKO mice (Fig. 3A–D). Immunohistochemistry for TNAP showed localization in odontoblasts and periodontal cells in WT, whereas *Col1a1*-cKO mice exhibited virtually no TNAP localization in the dentoalveolar complex (Fig. 3E–H). Picrosirius red staining confirmed a substantial loss of PDL collagen organization in *Col1a1*-cKO mice versus controls (Fig. 3I, K). TRAP staining revealed numerous osteoclast-like cells on alveolar bone surfaces in *Col1a1*-cKO mice (Fig. 3J, L), and enumeration showed a non-significant trend ($P > 0.05$; likely due to small sample size) of 4-fold increased osteoclast-like cells (Fig. 3M, N).

In the dentoalveolar tissues, *Prx1-Cre* deleter mice direct ablation to osteoblasts and other craniofacial mesenchyme (Logan et al. 2002). Cranial radiographs indicated mandibular incisor fracture and overgrowth of the maxillary incisor in some *Prx1*-cKO mice (Fig. 4A, B), possibly resulting from altered incisor material properties and/or malocclusion. Radiography and micro-CT of hemimandibles revealed that *Prx1*-cKO mouse mandibles featured relatively normal molars surrounded by reduced and radiolucent alveolar bone, as well as severely affected incisor root dentin (Fig. 4C–L). Quantitative micro-CT analysis indicated trends of decreased alveolar bone and crown and root dentin BV, BV/TV, and TMD in *Prx1*-cKO mice that did not reach significance ($P > 0.05$; Appendix Table 3). *Prx1*-cKO root dentin thickness was significantly decreased versus WT, though not as dramatically as in *Col1a1*-cKO mice. Three-dimensional reconstructions revealed dramatically reduced alveolar bone height in *Prx1*-cKO mice (Fig. 4M, N).

Histology of *Prx1*-cKO mice showed absence or reduction of acellular cementum, PDL detachment, and apical migration of junctional epithelium (Fig. 5A–D). Osteoid accumulation

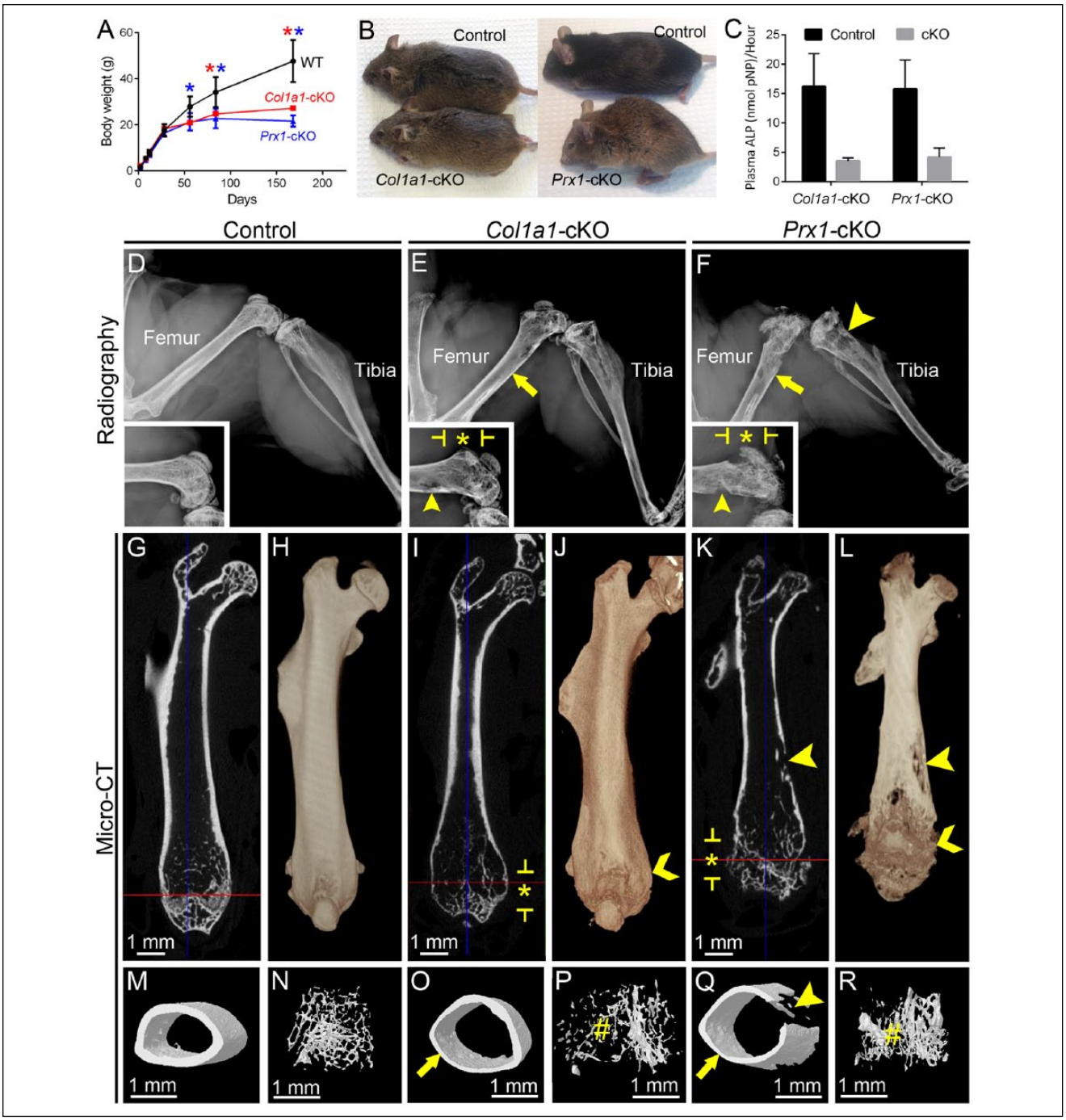


**Figure 1.** Conditional deletion of *Alpl* results in late-onset hypophosphatasia and associated skeletal disease. (**A**) Body weight for male and female WT and cKO mice ($n$ = 3 or 4 per genotype; shown as mean ± SD) was measured from 2 to 168 dpn (24 wk). Compared with WT, *Col1a1*-cKO mice (red line) showed significantly reduced (by independent samples $t$ test, $P < 0.05$) body weight at 84 and 168 dpn (red stars), while *Prx1*-cKO mice (blue line) showed significantly reduced body weight at 56, 84, and 168 dpn (blue stars). (**B**) Photographs of male mice at 24 wk, showing smaller body size of both cKO models versus WT. (**C**) Plasma alkaline phosphatase (ALP) activity measured at 24 wk indicates significant reductions of approximately 75% for both cKO models. (**D–F**) Radiographs of hind limbs from WT and cKO mice at 24 wk. Femora and tibiae from cKO mice exhibit radiolucency indicating hypomineralization, thin cortical bone (yellow arrows), radiolucent lesions (yellow arrowheads), deformation and widening (yellow chevrons), and disrupted growth plate and metaphyseal structures (starred regions indicated by yellow brackets). Insets show higher magnification of the distal region of the femur for control and cKO mice. Micro–computed tomography analysis of femora yielded (**G**, **I**, **K**) 2-dimensional orthogonal cross sections, (**H**, **J**, **L**) 3-dimensional volume renders, and 3-dimensional surface renders of (**M**, **O**, **Q**) cortical midshaft bone and (**N**, **P**, **R**) distal metaphyseal trabecular bone. Femora of cKO models exhibited thin cortical bone (yellow arrows), reduced and altered trabecular bone (yellow #), and radiolucent lesions (yellow arrowheads), and *Prx1*-cKO bones especially featured disrupted growth plate regions, many lesions (yellow arrowheads), surface degradation, and reduced length. Though a single representative WT control is shown here, proper controls that were age and background matched were used for qualitative and quantitative analyses of both *Col1a1*-cKO and *Prx1*-cKO mice. cKO, conditional knockout; dpn, days postnatal; WT, wild type.

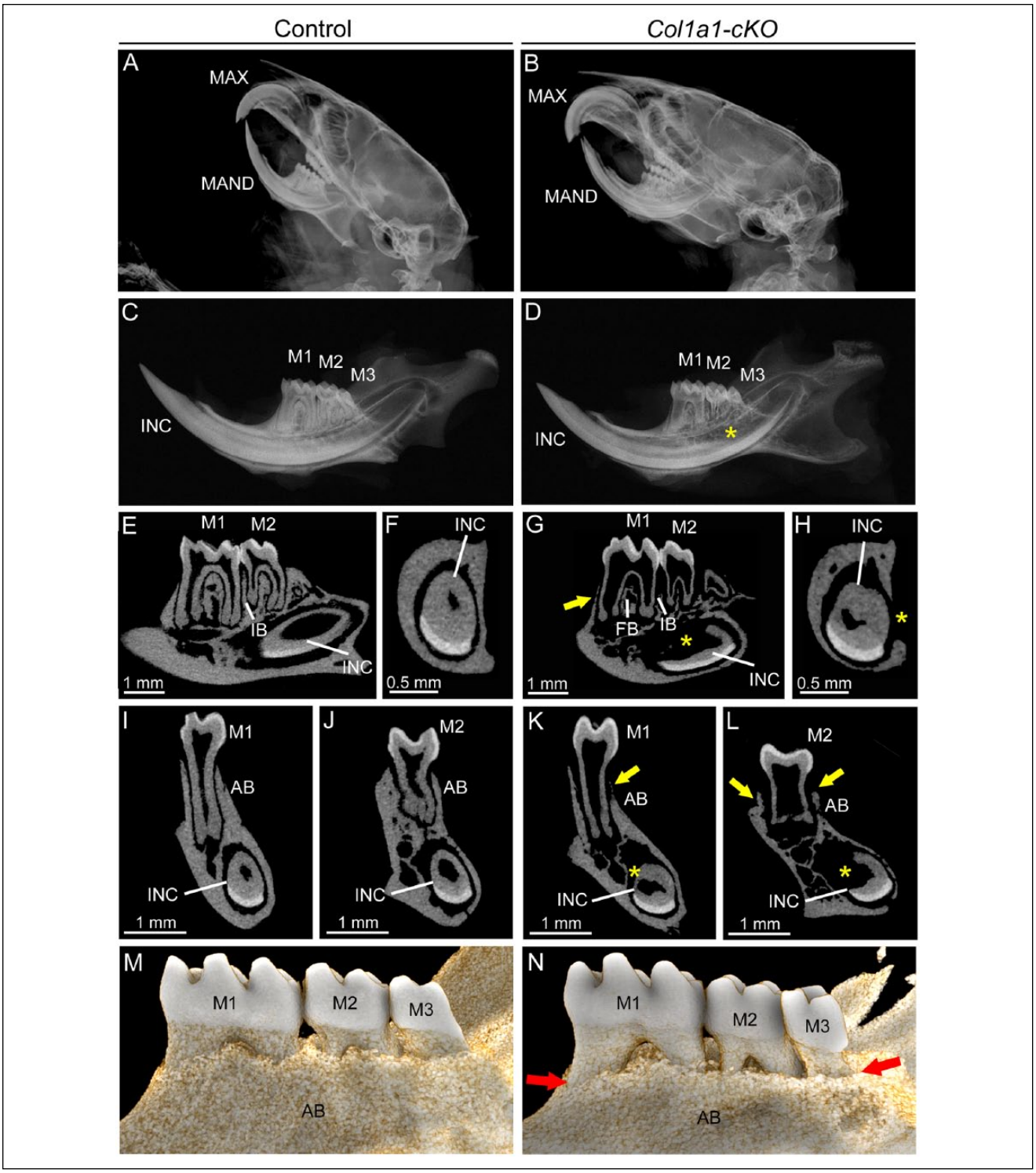


**Figure 2.** Mineralization defects in dentoalveolar tissues of *Col1a1*-cKO mice. Dentoalveolar tissues were analyzed by radiography and micro–computed tomography (micro-CT) in WT control and *Col1a1*-cKO mice ($n$ = 3 per genotype) at 24 wk. Compared with (**A**) WT crania, radiographs of (**B**) *Col1a1*-cKO mice indicate relatively normal anatomy and dental occlusion of incisors and molars of the maxilla (MAX) and mandible (MAN). However, compared with (**C**) controls, (**D**) *Col1a1*-cKO hemimandibles exhibit reduced mineralization of first through third molars (M1-M3), incisor (INC), and mandibular bone. By micro-CT, the well-mineralized tooth and bone structures of (**E**, **F**, **I**, **J**) WT mandibles are observed in (**G**, **H**, **K**, **L**) *Col1a1*-cKO mandibles to be severely defective, including reduced (yellow arrows) alveolar bone (AB) and loss of bone height in the furcation region (FB) and interproximal bone (IB) between molars. Molars feature short roots with thin dentin and widened pulp chambers as compared with controls. The lingual root analog dentin of the incisor is severely dysmorphic with delayed mineralization (yellow star). (**M**, **N**) Three-dimensional reconstructions of micro-CT scans reveal dramatically reduced lingual alveolar bone height (red arrows) in *Col1a1*-cKO mice, exposing roots surfaces of M1 to M3. cKO, conditional knockout; WT, wild type.

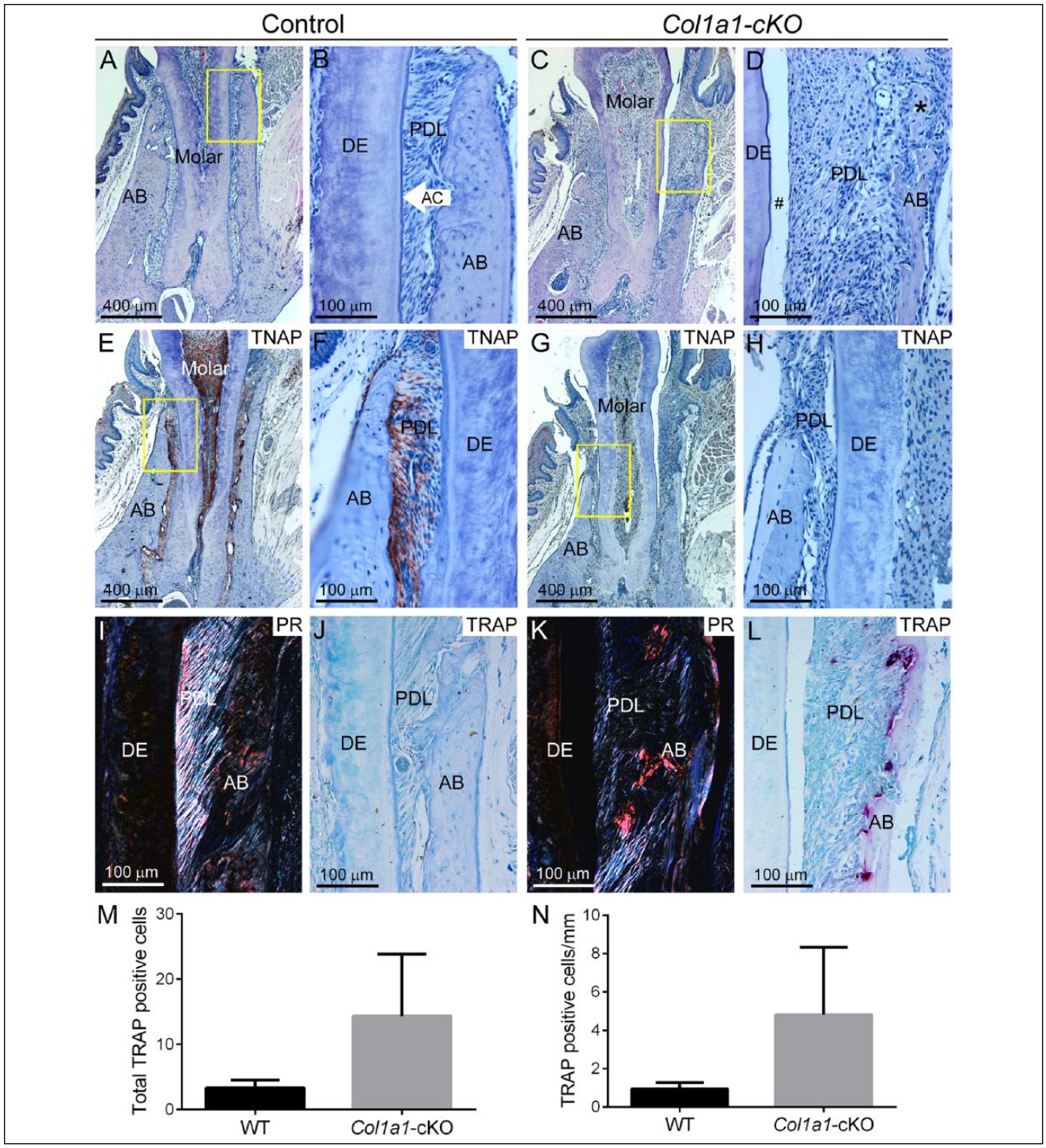


**Figure 3.** Defective dentin and periodontia in *Col1a1*-cKO mice. Dentoalveolar tissues were analyzed by histology in WT control and *Col1a1*-cKO mice ($n$ = 3 per genotype) at 24 wk. By histology, dentoalveolar structures of (**A**, **B**) WT molars—including alveolar bone (AB), acellular cementum (AC), periodontal ligament (PDL), and dentin (DE)—are organized and functional. (**C**, **D**) *Col1a1*-cKO mice exhibit thin and dysplastic dentin, lack of acellular cementum, PDL detachment (#), and osteoid accumulation at the alveolar bone crest (black stars). The yellow boxes (A, C) indicate regions of higher magnification (B, D, respectively). Immunohistochemistry for tissue nonspecific alkaline phosphatase (TNAP) in (**E**, **F**) WT shows localization in odontoblasts and periodontal cells, whereas (**G**, **H**) *Col1a1*-cKO mice exhibit no positive TNAP localization in the dentoalveolar complex. The yellow boxes (E, G) indicate regions of higher magnification (F, H, respectively). Picrosirius red (PR) staining in (**I**) WT highlights the highly organized collagen fibers of the PDL, while (**K**) this selective staining confirms a substantial loss of PDL collagen organization in *Col1a1*-cKO mice. Compared with the few osteoclast-like cells seen in (**J**) WT alveolar bone, tartrate-resistant acid phosphatase (TRAP) staining in (**L**) *Col1a1*-cKO mice reveals numerous osteoclast-like cells (large red-purple cells) on alveolar bone surfaces. Quantification and statistical analysis reveals a nonsignificant increase in (**M**) total numbers of TRAP-positive osteoclast-like cells, as well as (**N**) cells normalized to bone surface, in *Col1a1*-cKO vs. WT mice. cKO, conditional knockout; WT, wild type.

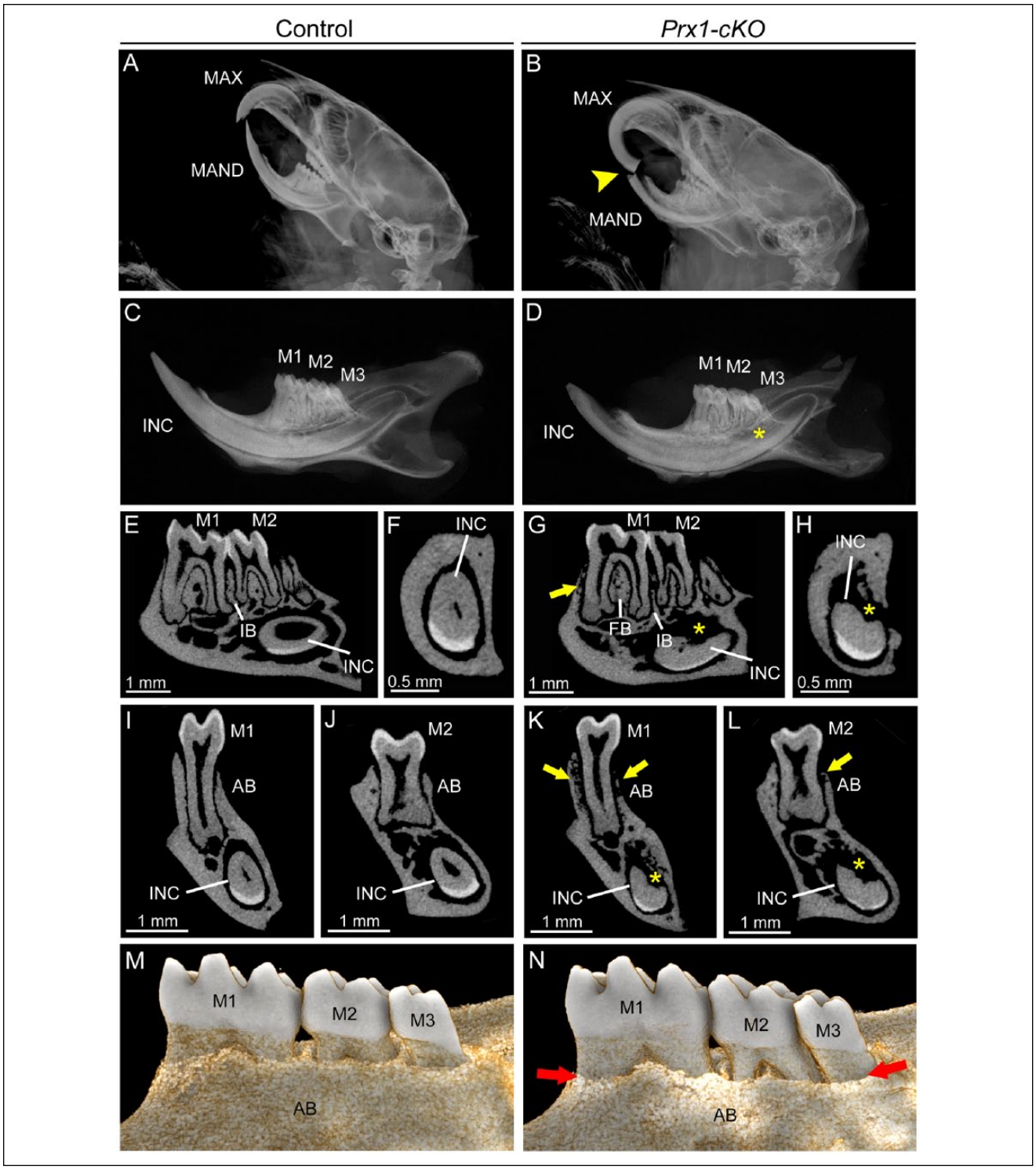


**Figure 4.** Mineralization defects in dentoalveolar tissues of *Prx1*-cKO mice. Dentoalveolar tissues were analyzed by radiography and micro–computed tomography (micro-CT) in WT control and *Prx1*-cKO mice ($n$ = 3 per genotype) at 24 wk. Compared with (**A**) WT crania, radiographs of (**B**) *Prx1*-cKO mice show mandibular incisor fracture and malocclusion (yellow arrowhead) of maxilla (MAX) and mandible (MAND). Compared with (**C**) WT hemimandibles, radiographs indicate that (**D**) *Prx1*-cKO mice feature reduced mineralization of bone and incisor (INC), although molars (M1-M3) appear relatively normal. By micro-CT, well-mineralized structures of the (**E**, **F**, **I**, **J**) WT mandible are observed in (**G**, **H**, **K**, **L**) *Prx1*-cKO mandibles to be defective, especially radiolucent and reduced regions (yellow arrows) of alveolar bone (AB) and reduction in bone height in the furcation region (FB) and interproximal bone (IB) between molars. Lingual root analogs of incisor teeth are severely defective (yellow *). (**M**, **N**) Three-dimensional reconstructions of micro-CT scans reveal dramatically reduced lingual alveolar bone height (red arrows) in *Prx1*-cKO mice, exposing roots surfaces of M1 to M3. cKO, conditional knockout; WT, wild type.

was observed on alveolar bone surfaces, especially the alveolar crest, where several hundred square micrometers of osteoid were typically observed. Radiolucent areas were observed to be a mix of unmineralized osteoid and resorbed bone, and PDL space was invaded by osteoid nearly to the point of ankylosis. In contrast to that of *Col1a1*-cKO mice, molar dentin appeared relatively normal in organization, whereas incisor root dentin was severely dystrophic. Immunohistochemistry showed that *Prx1*-cKO mice exhibited some residual TNAP at the alveolar bone border and in the PDL (Fig. 5E–H). Picrosirius red staining confirmed disorganization of PDL collagen in *Prx1*-cKO mice versus controls (Fig. 5I, K). TRAP staining revealed numerous osteoclast-like cells on *Prx1*-cKO alveolar bone surfaces (Fig. 5J, L), with a statistically significant 4-fold increase in total cells and cells normalized to alveolar bone surface versus WT (Fig. 5M, N).

## Discussion

To better model the long-term effects of HPP on skeletal and dentoalveolar tissues, we generated mice harboring a floxed *Alpl* allele. By crossing $Alpl^{fl/fl}$ mice with 2 distinct Cre recombinase mice, we generated 2 novel cKO models of late-onset HPP. Targeted deletion of *Alpl* in osteoblasts and selected dental-periodontal cells (*Col1a1*-cKO) or deletion in limb bud osteochondroprogenitors and craniofacial mesenchyme (*Prx1*-cKO) successfully phenocopied skeletal and dental aspects of HPP, without the epileptic seizures or early lethality associated with global *Alpl* knockout (Narisawa et al. 1997; Fedde et al. 1999). Both cKO mice displayed decreased body weight at adult ages, approximately 75% reduction in plasma ALP, and skeletal defects of HPP, including hypomineralization, hyperosteoidosis, rachitic changes, bone deformities and deterioration, reduced bone mineral density, and fractures. Both cKO models exhibited dentoalveolar defects, with *Col1a1*-cKO mice featuring classic signs of HPP, such as short molar roots, thin dentin, and periodontal defects, including lack of acellular cementum, PDL detachment, and hypomineralized alveolar bone. *Prx1*-cKO mice featured periodontal manifestations, but molar dentin development was less affected. Interestingly, both cKO mice exhibited dramatically reduced alveolar bone height consistent with periodontal disease. These novel models can inform on long-term skeletal and dental manifestations of HPP. Future uses of $Alp^{fl/fl}$ mice are anticipated to provide essential tools to further study etiopathologies of HPP, as well as therapeutic interventions.

### *Mouse Models of Late-Onset HPP*

The broad range of severity of human HPP spans from life-threatening forms (infantile and perinatal) to milder forms (prenatal benign, childhood, adult, and odontohypophosphatasia; Millan and Whyte 2016; Whyte 2016). Skeletal defects include rickets during growth and osteomalacia in adult life, bone deformities and deterioration, fractures, and bone pain. The $Alpl^{-/-}$ mouse has been essential for studying skeletal manifestations of infantile HPP (Narisawa et al. 1997; Fedde et al. 1999); however, its early lethality has prevented long-term studies. Crossing $Alpl^{fl/fl}$ mice with *Col1a1*-Cre mice (targeting osteoblasts in the skeleton) or *Prx1*-Cre mice (targeting limb bud mesenchyme, including osteochondroprogenitors) caused a 75% reduction in plasma ALP and recapitulated HPP skeletal defects in both models, including rickets, hypomineralization, bone deformations, spontaneous fractures, and qualitative and quantitative differences in cortical and trabecular bone compartments. Importantly, neither cKO model exhibited early lethality (living up to 6 mo in this study) or vitamin B6–dependent seizures (a hallmark of the most severe ALP deficiencies and early lethal forms of HPP), and gross body weight differences were not apparent until 8 to 12 wk old. These accumulated data support *Col1a1*- and *Prx1*-cKO mice as models of late-onset HPP, phenocopying key aspects of human juvenile and adult forms.

Despite arising from distinct Cre recombinase drivers, *Col1a1*- and *Prx1*-cKO mice feature similar phenotypes with an overlapping array of skeletal defects in cortical and trabecular bone. *Prx1*-cKO mouse long bones appeared more severely affected than those of *Col1a1*-cKO mice, exhibiting more severe rachitic changes to growth plates, more obvious reductions in size, deformations in shape, and surface degradations and lesions. Greater severity likely arises from osteoblast and chondrocyte compartments being targeted for *Alpl* ablation. For purposes of this proof-of-principle study, we elected to focus on confirmation that deletion of the floxed *Alpl* allele recapitulated HPP-associated skeletal defects. Future studies employing these and other Cre drivers will further elucidate how timing and/or tissue-specific deletion of *Alpl* contributes to severity of skeletal manifestations.

### *Dental Defects in Mouse Models of Late-Onset HPP*

Regardless of clinical type, the majority of HPP patients experience dental abnormalities (Foster, Nociti, et al. 2014; Foster, Ramnitz, et al. 2014; Bloch-Zupan 2016). Studies on $Alpl^{-/-}$ mice have defined etiologies of HPP-associated defects in alveolar bone, dentin, cementum, and enamel (Beertsen et al. 1999; Millán et al. 2008; McKee et al. 2011; Foster et al. 2012; Yadav et al. 2012; Foster, Nagatomo, et al. 2013; Gasque et al. 2015). However, early lethality of these mice limits analyses to developmental stages, precluding longer-term studies on tooth function, dentoalveolar remodeling, repair, and regeneration. One approach to resolve this limitation was creation of a knock-in mouse harboring a dominant-negative human *ALPL* mutation associated with odontohypophosphatasia (Hu et al. 2000; Silvent et al. 2014). $Alpl^{+/A116T}$ mice featured 50% reduced plasma ALP and no apparent skeletal defects, and they lived to be >1 y old (Foster et al. 2015). $Alpl^{+/A116T}$ mice showed alterations in dentoalveolar tissues, including hypomineralized alveolar bone and cellular cementum, and a trend of reduced acellular cementum. While these findings support $Alpl^{+/A116T}$ mice as a model of odontohypophosphatasia, limitations included lack of defects in dentin and enamel and a mildly affected periodontium.

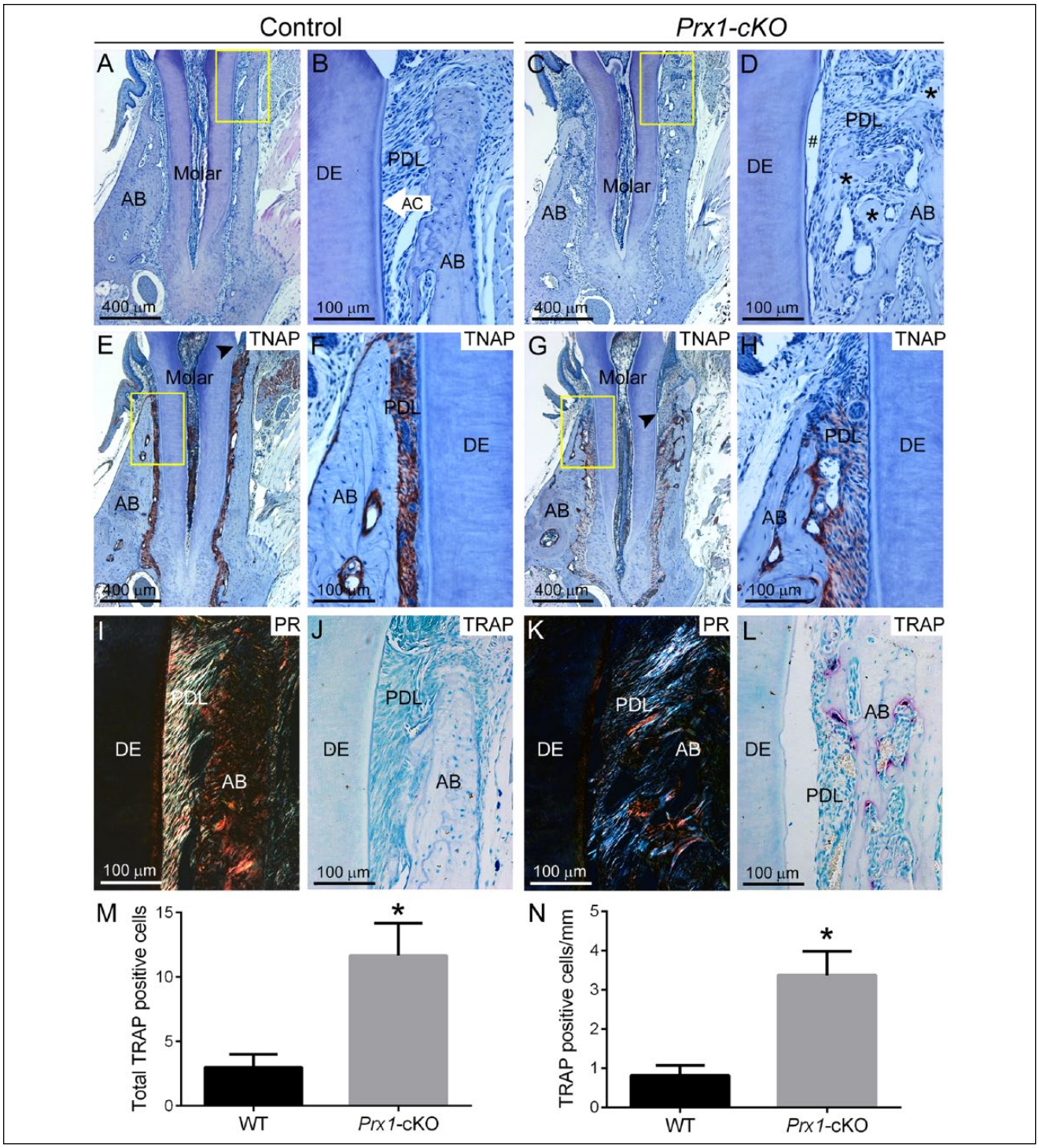


**Figure 5.** Defective periodontia in *Prx1*-cKO mice. Dentoalveolar tissues were analyzed by histology in WT control and *Prx1*-cKO mice ($n$ = 3 per genotype) at 24 wk. By histology, dentoalveolar structures of (**A**, **B**) WT molars—including alveolar bone (AB), acellular cementum (AC), periodontal ligament (PDL), and dentin (DE)—are organized and functional. (**C**, **D**) *Prx1*-cKO mice exhibit absence of the acellular cementum layer, PDL detachment (#), osteoid accumulation at the alveolar bone crest (black stars), and invasion of the PDL by alveolar bone. The yellow boxes (A, C) indicate regions of higher magnification (B, D, respectively). Immunohistochemistry for tissue nonspecific alkaline phosphatase (TNAP) in (**E**, **F**) WT shows localization in odontoblasts and periodontal cells, whereas (**G**, **H**) *Prx1*-cKO mice exhibit reduced TNAP localized mainly to the bone surface. Black arrowheads (E, G) indicate the location of junctional epithelium, revealing apical migration in *Prx1*-cKO mice. The yellow boxes (E, G) indicate regions of higher magnification (F, H, respectively). Picrosirius red (PR) staining in (**I**) WT highlights the highly organized collagen fibers of the PDL, while (**K**) this selective staining confirms a substantial loss of PDL collagen organization in *Prx1*-cKO mice. Compared with the few osteoclast-like cells seen in (**J**) WT alveolar bone, tartrate-resistant acid phosphatase (TRAP) staining in (**L**) *Prx1*-cKO mice reveals numerous osteoclast-like cells (large red-purple cells) on alveolar bone surfaces. Quantification and statistical analysis reveals a statistically significant (*$P$ < 0.05) increase in (**M**) total numbers of TRAP-positive osteoclast-like cells, as well as (**N**) cells normalized to bone surface, in *Prx1*-cKO vs. WT mice. cKO, conditional knockout; WT, wild type.

In dentoalveolar tissues, the *Col1a1*-Cre line targets gene ablation to type I collagen–producing cells, including odontoblasts, osteoblasts, cementoblasts, and fibroblasts (Dacquin et al. 2002; Kim et al. 2012; Kim et al. 2015). *Col1a1*-cKO mice recapitulated an array of classic human and mouse HPP dental defects, including short molar roots, thin dentin, widened pulp chambers, lack of acellular cementum, loss of attachment, and hypomineralized alveolar bone. Unique to the mouse, the *Col1a1*-cKO continually erupting incisor exhibited cementum defects and extremely dysmorphic and hypomineralized root analog dentin.

The *Prx1*-Cre line targets gene ablation to the craniofacial mesenchyme as well as limb buds (Lu et al. 1999; Logan et al. 2002). *Prx1* mRNA expression has been localized to the condensed ectomesenchyme surrounding mouse molar buds (Mitchell et al. 2006); however, its importance in later molar odontogenesis is less clear. In contrast, *Prx1* seems to have a critical role in initiating and patterning the mouse incisor (ten Berge et al. 1998). These developmental expression patterns become important in interpreting the dentoalveolar phenotype of *Prx1*-cKO mice in this study. *Prx1*-cKO mice exhibited relatively normal molar dentin (although micro-CT indicated reduced root dentin thickness) surrounded by a defective periodontium featuring acellular cementum defects, loss of attachment, and hypomineralized alveolar bone. Unlike molars, *Prx1*-cKO incisors featured hypomineralized and dysmorphic root analog dentin, resembling *Col1a1*-cKO mice in this respect. While *Prx1*-cKO mice do not recapitulate the full spectrum of severe HPP dental disease, they represent a point on the disease spectrum and may serve as a unique model for understanding periodontal defects independent of severely dysplastic dentin. Moreover, we believe that this report is the first to focus on the dentoalveolar phenotype arising from *Prx1*-Cre directed gene knockout, and these results may help direct future use of this mouse line in dental studies.

In both *Col1a1*- and *Prx1*-cKO models, we discovered increased osteoclast numbers on alveolar bone surfaces and severely reduced alveolar bone height. These characteristics, in combination with the observed cementum and PDL defects, are consistent with aspects of periodontal disease. While we did not analyze the presence of microbial infections, we noted no severe infiltration of neutrophils into the periodontia of either cKO model (data not shown). Periodontal disease has been reported in some HPP patients (Bloch-Zupan 2016; Foster, Ramnitz, et al. 2014; Rodrigues et al. 2012; Watanabe et al. 2001), although prevalence and etiology are not well described. The $Alpl^{+/A116T}$ mouse model also showed increased osteoclast numbers in alveolar bone, though periodontal function was maintained and alveolar bone loss not detected (Foster et al. 2015). Further study is required to understand mechanisms for increased osteoclasts and alveolar bone loss; however, these findings exemplify the novel insights and opportunities generated by these new HPP mouse models.

## Author Contributions

B.L. Foster, contributed to design, data acquisition, analysis, and interpretation, drafted and critically revised the manuscript; P. Kuss, contribute to conception, design, data acquisition, analysis, and interpretation, drafted and critically revised the manuscript; M.C. Yadav, contributed to conception, design, data acquisition, analysis, and interpretation, critically revised the manuscript; T.N. Kolli, contributed to data acquisition and analysis, critically revised the manuscript; S. Narisawa, contributed to conception, design, data acquisition, analysis, and interpretation, critically revised the manuscript; L. Lukashova, contributed to data acquisition, analysis, and critically revised manuscript; E. Cory, contributed to data acquisition, analysis, and interpretation, critically revised the manuscript; R.L. Sah, contributed to data acquisition, analysis, and interpretation, critically revised the manuscript; M.J. Somerman, contributed to data interpretation, critically revised the manuscript; J.L. Millán, contributed to conception, design, data acquisition, analysis, and interpretation, critically revised the manuscript. All authors gave final approval and agree to be accountable for all aspects of the work.

## Acknowledgments

This research was supported by grant DE 12889 to J.L.M. from the National Institute of Dental and Craniofacial Research of the National Institutes of Health (NIH); a research grant to B.L.F. from Soft Bones, Inc.; grant AR 066110 to B.L.F. from the National Institute of Arthritis and Musculoskeletal and Skin Diseases (NIAMS) / NIH; a fellowship to P.K. from the German Research Foundation; grant AG 007996 to R.L.S. from the National Institute of Aging / NIH; grant AR 046121 from NIAMS/NIH to the Hospital for Special Surgery; and the Intramural Research Program of NIAMS (M.J.S.). The authors thank Kenn Holmbeck (National Institute of Dental and Craniofacial Research) for assistance with micro–computed tomography analysis and Nasrin Kalantari Pour (NIAMS) for assistance with histology. The authors thank Diana Sandoval and the personnel at the Sanford Burnham Prebys Medical Discovery Institute animal facility for their assistance and careful animal husbandry. The authors declare no potential conflicts of interest with respect to the authorship and/or publication of this article.

## References

Beertsen W, VandenBos T, Everts V. 1999. Root development in mice lacking functional tissue non-specific alkaline phosphatase gene: inhibition of acellular cementum formation. J Dent Res. 78(6):1221–1229.

Bloch-Zupan A. 2016. Hypophosphatasia: diagnosis and clinical signs—a dental surgeon perspective. Int J Paediatr Dent. 26(6):426–438.

Bouxsein ML, Boyd SK, Christiansen BA, Guldberg RE, Jepsen KJ, Muller R. 2010. Guidelines for assessment of bone microstructure in rodents using micro-computed tomography. J Bone Miner Res. 25(7):1468–1486.

Dacquin R, Starbuck M, Schinke T, Karsenty G. 2002. Mouse alpha1(i)-collagen promoter is the best known promoter to drive efficient Cre recombinase expression in osteoblast. Dev Dyn. 224(2):245–251.

Fedde K, Blair L, Silverstein J, Coburn S, Ryan L, Weinstein R, Waymire K, Narisawa S, Millán J, MacGregor G, et al. 1999. Alkaline phosphatase knock-out mice recapitulate the metabolic and skeletal defects of infantile hypophosphatasia. J Bone Miner Res. 14(12):2015–2026.

Foster BL. 2012. Methods for studying tooth root cementum by light microscopy. Int J Oral Sci. 4(3):119–128.

Foster BL, Nagatomo KJ, Nociti FH Jr, Fong H, Dunn D, Tran AB, Wang W, Narisawa S, Millán JL, Somerman MJ. 2012. Central role of pyrophosphate in acellular cementum formation. PLoS One. 7(6):e38393.

Foster BL, Nagatomo KJ, Tso HW, Tran AB, Nociti FH Jr, Narisawa S, Yadav MC, McKee MD, Millan JI, Somerman MJ. 2013. Tooth root dentin mineralization defects in a mouse model of hypophosphatasia. J Bone Miner Res. 28(2):271–282.

Foster BL, Nociti FH Jr, Somerman MJ. 2014. The rachitic tooth. Endocr Rev. 35(1):1–34.

Foster BL, Ramnitz MS, Gafni RI, Burke AB, Boyce AM, Lee JS, Wright JT, Akintoye SO, Somerman MJ, Collins MT. 2014. Rare bone diseases and their dental, oral, and craniofacial manifestations. J Dent Res. 93(7):7S–19S.

Foster BL, Sheen CR, Hatch NE, Liu J, Cory E, Narisawa S, Kiffer-Moreira T, Sah RL, Whyte MP, Somerman MJ, et al. 2015. Periodontal defects in the a116t knock-in murine model of odontohypophosphatasia. J Dent Res. 94(5):706–714.

Foster BL, Soenjaya Y, Nociti FH, Holm E, Zerfas PM, Wimer HF, Holdsworth DW, Aubin JE, Hunter GK, Goldberg HA, et al. 2013. Deficiency in acellular cementum and periodontal attachment in Bsp null mice. J Dent Res. 92(2):166–172.

Gasque KC, Foster BL, Kuss P, Yadav MC, Liu J, Kiffer-Moreira T, van Elsas A, Hatch N, Somerman MJ, Millan JL. 2015. Improvement of the skeletal and dental hypophosphatasia phenotype in alpl(-/-) mice by administration of soluble (non-targeted) chimeric alkaline phosphatase. Bone. 72:137–147.

Hu J, Plaetke R, Mornet E, Zhang C, Sun X, Thomas H, Simmer J. 2000. Characterization of a family with dominant hypophosphatasia. Eur J Oral Sci. 108(3):189–194.

Kim TH, Bae CH, Jang EH, Yoon CY, Bae Y, Ko SO, Taketo MM, Cho ES. 2012. Col1a1-cre mediated activation of β-catenin leads to aberrant dentoalveolar complex formation. Anat Cell Biol. 45(3):193–202.

Kim TH, Bae CH, Lee JC, Kim JE, Yang X, de Crombrugghe B, Cho ES. 2015. Osterix regulates tooth root formation in a site-specific manner. J Dent Res. 94(3):430–438.

Limaye A. 2012. Drishti: a volume exploration and presentation tool. Paper presented at: SPIE—The International Society for Optical Engineering. San Diego, CA [accessed 2016 Jul 19]. https://www.researchgate.net/publication/265051079_Drishti_a_volume_exploration_and_presentation_tool_Proc_SPIE_8506_Developments_in_X-Ray_Tomography_VIII_85060X_October_17_2012.

Liu P, Zhang H, Liu C, Wang X, Chen L, Qin C. 2014. Inactivation of Fam20C in cells expressing type I collagen causes periodontal disease in mice. PLoS One. 9(12):e114396.

Logan M, Martin JF, Nagy A, Lobe C, Olson EN, Tabin CJ. 2002. Expression of Cre Recombinase in the developing mouse limb bud driven by a Prxl enhancer. Genesis. 33(2):77–80.

Lu M, Cheng H, Kern M, Potter S, Tran B, Diekwisch T, Martin J. 1999. Prx-1 functions cooperatively with another paired-related homeobox gene, Prx-2, to maintain cell fates within the craniofacial mesenchyme. Development. 126(3):495–504.

McKee MD, Nakano Y, Masica DL, Gray JJ, Lemire I, Heft R, Whyte MP, Crine P, Millan JL. 2011. Enzyme replacement therapy prevents dental defects in a model of hypophosphatasia. J Dent Res. 90(4):470–476.

Millán J. 2006. Alkaline phosphatases: structure, substrate specificity and functional relatedness to other members of a large superfamily of enzymes. Purinergic Signal. 2(2):335–341.

Millán J, Narisawa S, Lemire I, Loisel T, Boileau G, Leonard P, Gramatikova S, Terkeltaub R, Camacho N, McKee M, et al. 2008. Enzyme replacement therapy for murine hypophosphatasia. J Bone Miner Res. 23(6):777–787.

Millan JL, Whyte MP. 2016. Alkaline phosphatase and hypophosphatasia. Calcif Tissue Int. 98(4):398–416.

Mitchell JM, Hicklin DM, Doughty PM, Hicklin JH, Dickert JW Jr, Tolbert SM, Peterkova R, Kern MJ. 2006. The Prx1 homeobox gene is critical for molar tooth morphogenesis. J Dent Res. 85(10):888–893.

Narisawa S, Fröhlander N, Millán J. 1997. Inactivation of two mouse alkaline phosphatase genes and establishment of a model of infantile hypophosphatasia. Dev Dyn. 208(3):432–446.

Rodrigues TR, Georgetti AP, Martins L, Pereira Neto JS, Foster BL, Nociti FH Jr. 2012. Clinical correlate: case study of identical twins with cementum and periodontal defects resulting from odontohypophosphatasia. In: McCauley LK, Somerman MJ, editors. Mineralized tissues in oral and craniofacial science: Biological principles and clinical correlates. Ames, IA: Wiley-Blackwell. p. 183–190.

Silvent J, Gasse B, Mornet E, Sire JY. 2014. Molecular evolution of the tissue-nonspecific alkaline phosphatase allows prediction and validation of missense mutations responsible for hypophosphatasia. J Biol Chem. 289(35):24168–24179.

ten Berge D, Brouwer A, Korving J, Martin JF, Meijlink F. 1998. Prx1 and Prx2 in skeletogenesis: roles in the craniofacial region, inner ear and limbs. Development. 125(19):3831–3842.

Watanabe H, Hashimoto-Uoshima M, Goseki-Sone M, Orimo H, Ishikawa I. 2001. A novel point mutation (c571t) in the tissue-non-specific alkaline phosphatase gene in a case of adult-type hypophosphatasia. Oral Dis. 7(6):331–335.

Waymire KG, Mahuren JD, Jaje JM, Guilarte TR, Coburn SP, MacGregor GR. 1995. Mice lacking tissue non-specific alkaline phosphatase die from seizures due to defective metabolism of vitamin b-6. Nat Genet. 11(1):45–51.

Whyte MP. 2016. Hypophosphatasia: aetiology, nosology, pathogenesis, diagnosis and treatment. Nat Rev Endocrinol. 12(4):233–246.

Yadav MC, de Oliveira RC, Foster BL, Fong H, Cory E, Narisawa S, Sah RL, Somerman M, Whyte MP, Millán JL. 2012. Enzyme replacement prevents enamel defects in hypophosphatasia mice. J Bone Miner Res. 27(8):1722–1734.

Yadav MC, Lemire I, Leonard P, Boileau G, Blond L, Beliveau M, Cory E, Sah RL, Whyte MP, Crine P, et al. 2011. Dose response of bone-targeted enzyme replacement for murine hypophosphatasia. Bone. 49(2):250–256.

Zweifler LE, Patel MK, Nociti FH Jr, Wimer HF, Millán JL, Somerman MJ, Foster BL. 2015. Counter-regulatory phosphatases TNAP and NPP1 temporally regulate tooth root cementogenesis. Int J Oral Sci. 7(1):27–41.